1   **<u>Effects of Al grain size</u> on metal-induced layer exchange growth of**

2   **amorphous Ge thin film on glass substrate**

3

4   Mitsuki Nakata, Kaoru Toko*, and Takashi Suemasu

5

6   *Institute of Applied Physics, University of Tsukuba, 1-1-1 Tennodai, Tsukuba, Ibaraki*

7   *305-8573, Japan*

8

9

10   * Corresponding author: Kaoru Toko

11   Institute of Applied Physics, University of Tsukuba,

12   1-1-1 Tennohdai, Tsukuba, Ibaraki 305-8573, Japan

13   Phone: +81-29-853-5472, Fax: +81-29-853-5205

14   E-mail: toko@bk.tsukuba.ac.jp

15

16   **Abstract**

17   Metal-induced layer exchange (MILE) has attracted increasing attention as a way

18   to lower the crystallization temperature of amorphous semiconductor thin films on

19   insulating substrates. This paper demonstrates that the quality of the catalytic Al layer

20   strongly influences the growth properties in the MILE of amorphous Ge. The growth

21   velocity of the MILE significantly decreases with increasing the deposition temperature

22   of Al (T_{Al}: RT–200 °C), while the grain size of crystallized Ge becomes maximum (28

23   µm) at T_{Al} = 100 °C. This behavior is attributed to the Al grain size depending on T_{Al},

24   which influences both the nucleation frequency and the lateral growth velocity of Ge in

25   Al. These findings give new insight into MILE for fabricating high-quality

26   semiconductor thin films at low temperatures on inexpensive substrates.

27

28

29   **Keywords**: Metal-induced layer exchange; Al-induced crystallization; Solid phase

30   crystallization; Polycrystalline films; Semiconducting germanium

1. Introduction

Semiconductor thin film technology has been progressing rapidly for fabricating next-generation electronic devices with resource saving. Germanium is a promising candidate for a thin-film material because it has higher carrier mobilities than Si [1] and large light-absorbing capacity in the near-infrared [2]. Additionally, amorphous Ge (a-Ge) crystallizes at lower temperatures than the softening temperature of commonly-used glass (~550 °C) [3–5]. (111)-oriented Ge is particularly attractive because it provides a high carrier mobility for metal-oxide-semiconductor transistors [6,7] and acts as an epitaxial template for group III–V compound semiconductors [8,9], aligned nanowires [10,11], and spintronics materials [12]. These properties have motivated many researchers to synthesize orientation-controlled, large-grained Ge on glass for fabricating high-speed thin-film transistors, high-efficiency thin-film tandem solar cells, and multi-functional devices [13–17].

Highly (111)-oriented Ge layers have been recently achieved on glass [18–24] and plastic substrates [25–27] owing to the development of metal-induced layer exchange (MILE), that is, crystallization via the layer exchange between a-Ge and metals. The MILE is a powerful technique to fabricate high-speed thin-film transistors [28] or vertically aligned nanowires [29,30] on amorphous substrates including plastics.

The layer exchange phenomenon was originally found in the reaction between Al and Si [31–48]. The mechanism has been investigated over a decade from the perspective of both technological and scientific points, which is summarized as follows. The driving force of the MILE process is the difference in Gibbs energy between amorphous and crystalline Si [34,43–45]. First, Si atoms diffuse from metastable amorphous Si into Al through the Al grain boundaries (GBs) during annealing [42,43]. When the Si concentration in Al is supersaturated, Si nucleates in Al GBs [43,44]. After that, Si atoms dissolving in Al contact with the Si nuclei, which induces the lateral growth of Si crystals. The Si lateral growth stresses Al and pushing it to the upper layer [42,43]. Eventually, Si forms a bottom layer while Al forms an upper layer. The crystal quality of the resulting Si layer depends on the growth rate, i.e., the Si diffusion rate into Al [47,48].

The abovementioned mechanism is applicable to MILE between Ge and Al. Because the MILE begins with the diffusion of Ge atoms into Al GBs, the Al grain size should influence the MILE process and also the crystal quality of the resulting poly-Ge layer. In the present study, we therefore focus on the effects of the initial Al grain size on the MILE process of a-Ge. We demonstrate that the Al grain size has an optimum value for providing Ge of good crystal quality.

67

2. Experimental details

Fig. 1 presents a schematic of the sample preparation process. We prepared 50-nm-thick Al layers on SiO_2 glass substrates where the substrate temperatures (T_{Al}) were room temperature (RT), 50 °C, 100 °C, and 200 °C. After natural cooling, the Al layers were exposed to air for 5 min to form native AlO_x membranes as diffusion-limiting layers. Because the MILE progresses with the diffusion of Ge into Al as mentioned above, the diffusion-limiting layer significantly influences the growth properties of the MILE [19,22,37]. Then, 40-nm-thick a-Ge layers were prepared on the AlO_x at RT. Here, the thickness of the a-Ge layers is thinner than that of the Al layers in order to clarify growth domains [21]. All of the depositions were performed using radio frequency (RF) magnetron sputtering (Sanyu Electron SVC-700RF, base pressure: 3.0 × 10^{-4} Pa) with an Ar pressure of 0.2 Pa and an RF power of 50 W. The deposition rate was 28 nm min^{-1} for Ge and 31 nm min^{-1} for Al. Finally, the samples were annealed at 385 °C in N_2 for 1–100 h to induce layer exchange between Ge and Al. The semiconductor layer grown by MILE does not contain N atoms after annealing [19,40]. The samples were evaluated using Nomarski optical microscopy (Leica DM 2500 M), atomic force microscopy (AFM, SHIMADZU SPM-9600), and electron backscatter

85 diffraction (EBSD, TSL OIM analysis).

86

3. Results and discussion

88   The grain size of the as-deposited Al layers were roughly evaluated using AFM.

89 The results are shown in Fig. 2. As shown in the AFM images, the surface of the Al

90 layers takes on different forms depending on T_{Al}. The average grain size of Al,

91 estimated from the AFM images, clearly increases with increasing T_{Al}. This behavior is

92 common in sputtering deposition [49].

93   We evaluated the growth velocity of crystalline Ge in the MILE process as a

94 function of T_{Al} using Nomarski optical microscopy observing the back surface of the

95 samples. The growth evolution for the sample with $T_{Al} = 100$ °C is shown in Fig.

96 3(a)–(c), where the dark-colored area indicates crystallized Ge and the bright-colored

97 area indicates Al. The micrographs indicate that crystal Ge domains laterally grow with

98 increasing annealing time. As shown in Fig. 3(c), the lateral growth stops before the

99 growth fronts collide with each other because the initial Ge is thinner than Al [21].

100   We measured the Ge domain sizes (diameters) from Nomarski optical

101 micrographs for the samples with $T_{Al} = $ RT, 50 °C, 100 °C and 200 °C. The results are

102 summarized in Fig. 3(d) as a function of the annealing time. For all samples except T_{Al}

103   = 200 °C, the domain size increases as the annealing time increases and becomes

104   saturated. We note that the higher T_{Al} provided the larger saturated domain size. For the

105   sample with T_{Al} = 200 °C, the domain growth was not saturated within 100 h. The

106   lateral growth velocity of the Ge domains can be derived from the slopes in Fig. 3(d)

107   because the lateral growth velocity in MILE is almost consistent with annealing time

108   [47,48]. Fig. 3(e) shows the lateral growth velocity of the Ge domains as a function of

109   T_{Al}. It is found that the growth velocity clearly decreases with an increase of T_{Al}. This

110   behavior will be discussed later together with the crystal quality of Ge.

111   In MILE, a growth domain is generally divided into several grains [19,27]. The

112   actual grain sizes of the resulting Ge layers were evaluated using EBSD analysis. Before

113   EBSD, top Al layers were removed using an HF solution (HF: 1.5%) for 1 min. Fig.

114   4(a)–(d) show that the crystal orientation of Ge strongly depends on T_{Al}: the (111)

115   orientation fraction is maximum for the sample with T_{Al} = 100 °C. Such (111)

116   orientation can be explained from the perspective of the appearance of the energetically

117   stable plane [18,44]. In MILE, the lower growth rate leads to the higher (111) fraction

118   [19,40,47,48]. On the other hand, the (111) fraction decreases with increasing the

119   surface roughness of Al [46,48]. The sample with T_{Al} = 100 °C presented the highest

120   (111) fraction among the samples in this study likely owing to the good balance between

121   the growth rate and the surface roughness of Al. The grain size of Ge was defined as the

122   diameter of the regions surrounded by the black solid lines in Fig. 4(a)–(d). Fig. 4(e)

123   shows the grain size of Ge quantitatively calculated from the EBSD analysis software.

124   The grain size of Ge also has a peak at T_{Al} = 100 °C. These results mean that T_{Al} has an

125   optimum value for providing Ge of good crystal quality while the growth velocity

126   monotonically decreases with increasing T_{Al}. It is difficult to exclude the possibility of

127   impurity contamination in Al: the small grain size of the sample with T_{Al} = 200 °C could

128   be attributed to the chemical reactions with vacuum impurities (e.g., O, hydrocarbons,

129   etc.) during the high temperature deposition of Al. However, the T_{Al} dependence of the

130   Ge grain size can be explained as follows from the perspective of the effects of the Al

131   grain size on the nucleation frequency and lateral growth velocity of Ge.

132   Fig. 5 schematically shows the cross-section of Al during annealing. In MILE, Ge

133   atoms diffuse into Al GBs, followed by lattice diffusion [39–42]. When the Ge

134   concentration in Al reaches the solubility limit, Ge nucleates [44]. The more Al GBs

135   therefore provides the higher nucleation frequency. On the other hand, the lateral growth

136   of Ge proceeds by ingesting Ge atoms dissolved in Al, especially in Al GBs. Therefore,

137   the more Al GBs provides the higher lateral growth velocity. When T_{Al} is low ($\leq$ 50 °C),

138   the Al grain size is small (~120 nm) [Fig. 5(a)]. This provides a high Ge nucleation

139 frequency, resulting in small Ge grains (~40 μm) [Fig. 5(b)]. When T_{Al} is medium (~

140 100 °C), the Al grain size is medium (~140 nm) [Fig. 5(c)]. In this case, the lateral

141 growth velocity is relatively high compared to the nucleation frequency, resulting in

142 large Ge grains (~60 μm) [Fig. 5(d)]. When T_{Al} is high (> 200 °C), the Al grain size is

143 large (~160 nm) [Fig. 5(e)]. This makes a lateral growth slow, and then another

144 nucleation occurs before the lateral growth ingest Ge atoms in Al GBs [Fig. 5(f)]. This

145 behavior results in small Ge grains (~20 μm). Thus, the Ge grain size and growth

146 velocity in MILE strongly depend on the Al grain size.

147

148 **4. Conclusion**

149 We investigated the effects of Al quality on the MILE of a-Ge. The Al grain size

150 varied (120–160 nm) depending on the deposition temperature T_{Al} (RT–200 °C). The

151 growth velocity of MILE decreased with increasing T_{Al}, while the grain size of Ge

152 became maximum at T_{Al} = 100 °C. This behavior was explained from the perspective of

153 the nucleation frequency and lateral growth velocity depending on the Al grain size.

154 These findings give new insight into metal-induced crystallization for fabricating

155 high-quality semiconductor thin films on insulating substrates at low temperatures.

156

162 **References**

163 [1] J.C. Irvin, S.M. Sze, Resistivity, mobility and impurity levels in GaAs, Ge, and Si at 300 degrees,

164   Solid. State. Electron. 11 (1968) 599–602.

165 [2] W. Dash, R. Newman, Intrinsic Optical Absorption in Single-Crystal Germanium and Silicon at

166   77°K and 300°K, Phys. Rev. 99 (1955) 1151–1155.

167 [3] K. Toko, I. Nakao, T. Sadoh, T. Noguchi, M. Miyao, Electrical properties of poly-Ge on glass

168   substrate grown by two-step solid-phase crystallization, Solid-State Electron. 53 (2009) 1159.

169 [4] C.-Y. Tsao, J.W. Weber, P. Campbell, G. Conibeer, D. Song, M. A. Green, In situ low temperature

170   growth of poly-crystalline germanium thin film on glass by RF magnetron sputtering, Sol. Energy

171   Mater. Sol. Cells. 94 (2010) 1501–1505.

172 [5] M. Tada, J.-H. Park, D. Kuzum, G. Thareja, J.R. Jain, Y. Nishi, K.C. Saraswat, Low Temperature

173   Germanium Growth on Silicon Oxide Using Boron Seed Layer and In Situ Dopant Activation, J.

174   Electrochem. Soc. 157 (2010) H371–H376.

175 [6] T. Sanada, Y. Nakakita, M. Takenaka, S. Takagi, Surface orientation dependence of interface

176   properties of GeO_2/Ge metal-oxide-semiconductor structures fabricated by thermal oxidation, J.

177   Apply. Phys. 106 (2009) 073716.

178 [7] T. Nishimura, L.H. Lee, T. Tabata, S.K. Wang, K. Nagashio, K. Kita, A. Toriumi,

179   High-Electron-Mobility Ge n-Channel Metal-Oxide-Semiconductor Field-Effect Transistors with

180   High-Pressure Oxidized Y_2O_3, Appl. Phys. Express 4 (2011) 064201.

181   [8] T. Kawai, H. Yonezu, H. Yoshida, K. Pak, Ge segregation and its suppression in GaAs epilayers

182   grown on Ge(111) substrate, Appl. Phys. Lett. 61 (1992) 1216–1218.

183   [9] R.R. Lieten, S. Degroote, K. Cheng, M. Leys, M. Kuijk, G. Borghs, Growth of GaN on Ge(111)

184   by molecular beam epitaxy, Appl. Phys. Lett. 89 (2006) 252118.

185   [10] E.P.M. Bakkers, J. Dam, S. Franceschi, L.P. Kouwenhoven, M. Kaiser, M. Verheijen, H.

186   Wondergem, P. Sluis, Epitaxial growth of InP nanowires on germanium, Nat. Mater. 3 (2004) 769.

187   [11] N. Fukata, K. Sato, M. Mitome, Y. Band, T. Sekiguchi, M. Kirkham, J.I. Hong, Z.L. Wang, R.L.

188   Snyder, Doping and Raman Characterization of Boron and Phosphorus Atoms in Germanium

189   Nanowires, ACS Nano 4 (2010) 3807.

190   [12] K. Hamaya, H. Itoh, O. Nakatuka, K. Ueda, K. Yamamoto, M. Itakura, T. Taniyama, T. Ono, M.

191   Miyao, Ferromagnetism and Electronic Structures of Nonstoichiometric Heusler-Alloy $Fe_{3-x}Mn_xSi$

192   Epilayers Grown on Ge(111), Phys. Rev. Lett. 102 (2009) 137204.

193   [13] K. Toko, H. Kanno, A. Kenjo, T. Sadoh, T. Asano, M. Miyao, Ni-imprint induced solid-phase

194   crystallization in $Si_{1-x}Ge_x$ (x: 0–1) on insulator, Appl. Phys. Lett. 91 (2007) 042111.

195   [14] J.-H. Park, P. Kapur, K.C. Saraswat, H. Peng, A very low temperature single crystal germanium

196   growth process on insulating substrate using Ni-induced lateral crystallization for

197   three-dimensional integrated circuits, Appl. Phys. Lett. 91 (2007) 143107.

198   [15] K. Sakaike, S. Higashi, H. Murakami, S. Miyazaki, Crystallization of amorphous Ge films

199   induced by semiconductor diode laser annealing, Thin Solid Films. 516 (2008) 3595–3600.

200   [16] M. Uenuma, B. Zhenga, T. Imazawa, M. Horita, T. Nishidaa, Y. Ishikawa, Y. Uraoka,

201   Metal-nanoparticle-induced crystallization of amorphous Ge film using ferritin, Appl. Surf. Sci.

202   258 (2012) 3410–3414.

203   [17] E. Kim, S.-W. Moon, W.-W. Park, S.-H. Han, Growth of preferred orientation Ge film using

204   inductively coupled plasma-assisted DC magnetron sputtering at low temperature, Thin Solid Films.

205   548 (2013) 186–189.

206   [18] S. Hu, A.F. Marshall, P.C. McIntyre, Interface-controlled layer exchange in metal-induced

207   crystallization of germanium thin films, Appl. Phys. Lett. 97 (2010) 082104.

208   [19] K. Toko, M. Kurosawa, N. Saitoh, N. Yoshizawa, N. Usami, M. Miyao, T. Suemasu, Highly

209   (111)-oriented Ge thin films on insulators formed by Al-induced crystallization, Appl. Phys. Lett.

210   101 (2012) 072106.

211   [20] J.-H. Park, T. Suzuki, M. Kurosawa, M. Miyao, T. Sadoh, Nucleation-controlled

212   gold-induced-crystallization for selective formation of Ge(100) and (111) on insulator at

213   low-temperature (~250 °C), Appl. Phys. Lett. 103 (2013) 082102.

214   [21] K. Nakazawa, K. Toko, N. Saitoh, N. Yoshizawa, N. Usami, T. Suemasu, Large-Grained

215   Polycrystalline (111) Ge Films on Insulators by Thickness-Controlled Al-Induced Crystallization,

216   ECS J. Solid State Sci. Technol. 2 (2013) Q195–Q199.

217   [22] K. Toko, R. Numata, N. Oya, N. Fukata, N. Usami, T. Suemasu, Low-temperature (180 °C)

218   formation of large-grained Ge (111) thin film on insulator using accelerated metal-induced

219   crystallization, Appl. Phys. Lett. 104 (2014) 022106.

220   [23] P. Wang, X. Li, H. Liu, S. Lai, Y. Chen, Y. Xu, S. Chen, C. Li, W. Huang, D. Tang, High (111)

221   orientation poly-Ge film fabricated by Al induced crystallization without the introduction of AlO_x

222   interlayer, Mater. Res. Bull. 72 (2015) 60–63.

223   [24] H. Okamoto, K. Kudo, T. Nomitsu, R. Mochii, K. Moto, K. Takakura, I. Tsunoda, Au induced

224   low-temperature formation of preferentially (111)-oriented crystalline Ge on insulator, Jpn. J. Appl.

225   Phys. 55 (2016) 04EJ10.

226   [25] J.H. Park, K. Kasahara, K. Hamaya, M. Miyao, T. Sadoh, High carrier mobility in

227   orientation-controlled large-grain ($\geq$50 μm) Ge directly formed on flexible plastic by

228   nucleation-controlled gold-induced-crystallization, Appl. Phys. Lett. 104 (2014) 252110.

229   [26] N. Oya, K. Toko, N. Saitoh, N. Yoshizawa, T. Suemasu, Direct synthesis of highly textured Ge

230   on flexible polyimide films by metal-induced crystallization, Appl. Phys. Lett. 104 (2014) 262107.

231   [27] H. Higashi, K. Kasahara, K. Kudo, H. Okamoto, K. Moto, J.-H. Park, S. Yamada, T. Kanashima,

232   M. Miyao, I. Tsunoda, and K. Hamaya, A pseudo-single-crystalline germanium film for flexible

233   electronics, Appl. Phys. Lett. 106 (2015) 041902.

234   [28] K. Kasahara, Y. Nagatomi, K. Yamamoto, H. Higashi, M. Nakano, S. Yamada, D. Wang, H.

235   Nakashima, K. Hamaya, Electrical properties of pseudo-single-crystalline germanium

236   thin-film-transistors fabricated on glass substrates, Appl. Phys. Lett. 107 (2015) 142102.

237   [29] M. Nakata, K. Toko, W. Jevasuwan, N. Fukata, N. Saitoh, N. Yoshizawa, T. Suemasu,

238   Transfer-free synthesis of highly ordered Ge nanowire arrays on glass substrates, Appl. Phys. Lett.

239   107 (2015) 133102.

240   [30] K. Toko, M. Nakata, W. Jevasuwan, N. Fukata, T. Suemasu, Vertically Aligned Ge Nanowires

241   on Flexible Plastic Films Synthesized by (111)-Oriented Ge Seeded Vapor-Liquid-Solid Growth,

242   ACS Appl. Mater. Interfaces. 7 (2015) 18120–18124.

243   [31] O. Nast, T. Puzzer, L.M. Koschier, A.B. Sproul, S.R. Wenham, Aluminum-induced

244   crystallization of amorphous silicon on glass substrates above and below the eutectic temperature,

245   Appl. Phys. Lett. 73 (1998) 3214.

246   [32] S. Gall, M. Muske, I. Sieber, O. Nast, W. Fuhs, Aluminum-induced crystallization of amorphous

247   silicon, J. Non. Cryst. Solids. 299–302 (2002) 741–745.

248   [33] N.-P. Harder, T. Puzzer, P.I. Widenborg, S. Oelting, A.G. Aberle, Ion-Assisted Low-Temperature

249   Silicon Epitaxy on Randomly Textured Seed Layers on Glass, Cryst. Growth Des. 3 (2003)

250   767–771.

251   [34] J. Schneider, a. Schneider, a. Sarikov, J. Klein, M. Muske, S. Gall, et al., Aluminum-induced

252   crystallization: Nucleation and growth process, J. Non. Cryst. Solids. 352 (2006) 972–975.

253   [35] D. Van Gestel, M.J. Romero, I. Gordon, L. Carnel, J. D'Haen, G. Beaucarne, M. Al-Jassim, J.

254   Poortmans, Electrical activity of intragrain defects in polycrystalline silicon layers obtained by

255   aluminum-induced crystallization and epitaxy, Appl. Phys. Lett. 90 (2007) 092103.

256   [36] K.Y. Lee, C. Becker, M. Muske, F. Ruske, S. Gall, B. Rech, M. Berginski, J. Hüpkes,

257   Temperature stability of ZnO:Al film properties for poly-Si thin-film devices, Appl. Phys. Lett. 91

258   (2007) 241911.

259   [37] M. Kurosawa, N. Kawabata, T. Sadoh, M. Miyao, Orientation-controlled Si thin films on

260   insulating substrates by Al-induced crystallization combined with interfacial-oxide layer

261   modulation, Appl. Phys. Lett. 95 (2009) 132103.

262   [38] C. Jaeger, M. Bator, S. Matich, M. Stutzmann, Two-step crystallization during the reverse

263   aluminum-induced layer exchange process, J. Appl. Phys. 108 (2010) 113513.

264   [39] R. Numata, K. Toko, N. Saitoh, N. Yoshizawa, N. Usami, T. Suemasu, Orientation Control of

265   Large-Grained Si Films on Insulators by Thickness-Modulated Al-Induced Crystallization, Cryst.

266   Growth Des. 13 (2013) 1767–1770.

267   [40] K. Toko, R. Numata, N. Saitoh, N. Yoshizawa, N. Usami, T. Suemasu, Selective formation of

268   large-grained, (100)- or (111)-oriented Si on glass by Al-induced layer exchange, J. Appl. Phys. 115

269   (2014) 094301.

270   [41] Y. Sugimoto, N. Takata, T. Hirota, K. Ikeda, F. Yoshida, H. Nakashima, H. Nakashima,

271   Low-Temperature Fabrication of Polycrystalline Si Thin Film Using Al-Induced Crystallization

272   without Native Al Oxide at Amorphous Si/Al Interface, Jpn. J. Appl. Phys. 44 (2005) 4770–4775.

273   [42] B.I. Birajdar, T. Antesberger, B. Butz, M. Stutzmann, E. Spiecker, Direct in situ transmission

274   electron microscopy observation of Al push up during early stages of the Al-induced layer

275   exchange, Scripta Materialia 66 (2012) 550.

276   [43] Z. Wang, L. Gu, L.P.H. Jeurgens, F. Phillipp, E.J. Mittemeijer, Real-time visualization of

277   convective transportation of solid materials at nanoscale., Nano Lett. 12 (2012) 6126–32.

278   [44] A. Sarikov, J. Schneider, J. Berghold, M. Muske, I. Sieber, S. Gall, W. Fuhs, A kinetic

279   simulation study of the mechanisms of aluminum induced layer exchange process, J. Appl. Phys.

280   107 (2010) 114318.

281   [45] D. Van Gestel, I. Gordon, J. Poortmans, Aluminum-induced crystallization for thin-film

282   polycrystalline silicon solar cells: Achievements and perspective, Sol. Energy Mater. Sol. Cells.

283   119 (2013) 261–270.

284   [46] C. Kendrick, C. Bomberger, N. Dawley, J. Georgiev, H. Shen, J.M. Redwing, Silicon nanowire

285   growth on poly-silicon-on-quartz substrates formed by aluminum-induced crystallization, Cryst.

286   Res. Technol. 48 (2013) 658–665.

287   [47] N. Usami, M. Jung, T. Suemasu, On the growth mechanism of polycrystalline silicon thin film

288   by Al-induced layer exchange process, J. Cryst. Growth. 362 (2013) 16–19.

289   [48] M. Kurosawa, T. Sadoh, M. Miyao, Comprehensive study of Al-induced layer-exchange growth

290   for orientation-controlled Si crystals on SiO_2 substrates, J. Appl. Phys. 116 (2014) 173510.

291   [49] J.A. Thornton, Influence of apparatus geometry and deposition conditions on the structure and

292   topography of thick sputtered coatings, J. Vac. Sci. Technol. 11 (1974) 666.

293

294

295 **Figure captions**

296

297 **Fig. 1.** Illustration of the process of Al-induced layer exchange growth of a-Ge on a

298 glass substrate.

299

300

301 **Fig. 2.** Average grain size of the as-deposited Al layers as a function of T_{Al}. The grain

302 size was estimated from AFM images, as typical shown for the samples with $T_{Al} = \text{RT}$

303 and 200 °C.

304

305

306 **Fig. 3.** (a-c) Nomarski optical micrographs showing the back surface of the sample with

307 $T_{Al} = 100$ °C through the transparent substrate, where the sample was annealed at

308 385 °C for (a) 5 h, (b) 10 h, and (c) 50 h. (d) Annealing time dependence of the size

309 (diameter) of crystalline Ge domains, estimated from Nomarski optical micrographs, for

310 the samples with $T_{Al} = \text{RT}$, 50, 100, and 200 °C. (e) Lateral growth velocity of the Ge

311 domains as a function of T_{Al}.

312

313 **Fig. 4.** (a-d) EBSD images of the samples with T_{Al} = (a) RT, (b) 50, (c) 100, and (d)

314 200 °C, taken from the normal direction relative to the sample substrates. The coloration

315 indicates crystal orientation, as shown in the legend. <u>The black solid lines in the EBSD</u>

316 <u>images indicate random grain boundaries.</u> (e) Average grain size of Ge calculated from

317 EBSD analyses as a function of T_{Al}.

318

319 **Fig. 5.** Schematic presentation of the MILE process depending on the Al grain size,

320 showing the cross-section of the Al layers during annealing where the Al grain size is
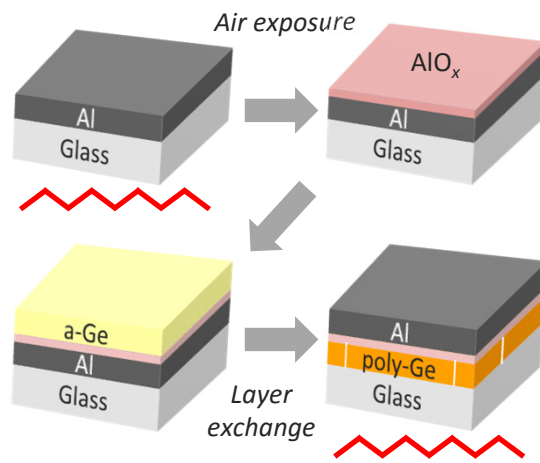
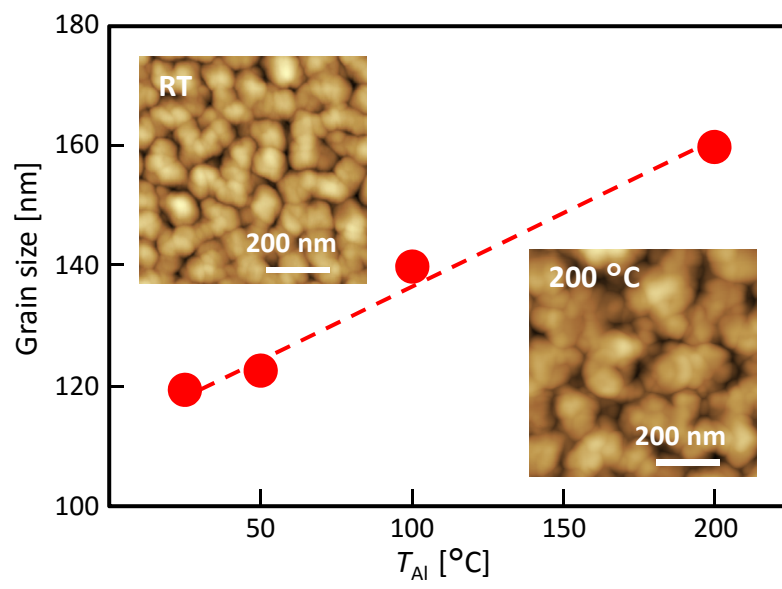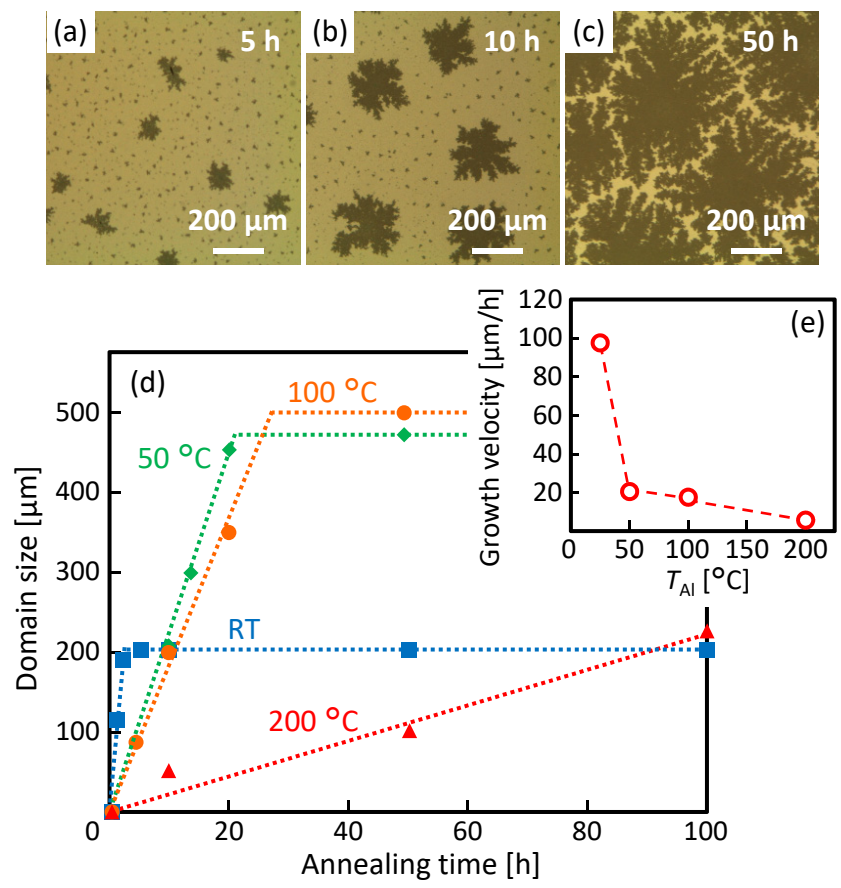321 (a,b) small, (c,d) medium, and (e,f) large.

322

Fig. 1

Fig. 2

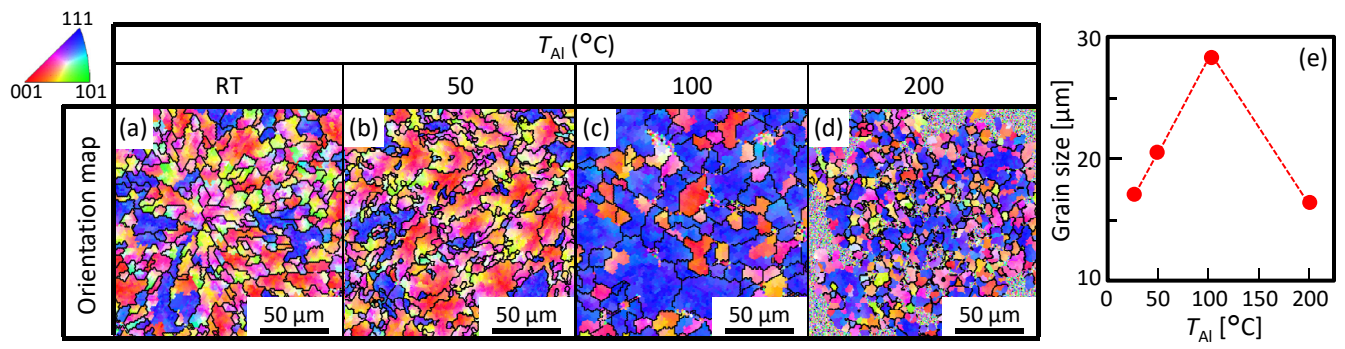(a) 5 h   200 µm
(b) 10 h   200 µm
(c) 50 h   200 µm

(d)

100 °C
50 °C
RT
200 °C

Domain size [µm]

Annealing time [h]

(e)

Growth velocity [µm/h]

T_{Al} [°C]

Fig. 3

Fig. 4

Al grain boundary **Crystalline Ge** **Dissolved Ge**

(a) Al grain size: small

(b) Ge grain size: small

(c) Al grain size: medium

(d) Ge grain size: large

(e) Al grain size: large

(f) Ge grain size: small

Fig. 5